

REPORT DOCUMENTATION PAGE

Form Approved
OMB No. 0704-0188

Public reporting burden for this collection of information is estimated to average 1 hour per response, including the time for reviewing instructions, searching existing data sources, gathering and maintaining the data needed, and completing and reviewing this collection of information. Send comments regarding this burden estimate or any other aspect of this collection of information, including suggestions for reducing this burden to Department of Defense, Washington Headquarters Services, Directorate for Information Operations and Reports (0704-0188), 1215 Jefferson Davis Highway, Suite 1204, Arlington, VA 22202-4302. Respondents should be aware that notwithstanding any other provision of law, no person shall be subject to any penalty for failing to comply with a collection of information if it does not display a currently valid OMB control number. **PLEASE DO NOT RETURN YOUR FORM TO THE ABOVE ADDRESS.**

1. REPORT DATE (DD-MM-YYYY) 29-11-2010		2. REPORT TYPE Journal Article		3. DATES COVERED (From - To)	
4. TITLE AND SUBTITLE A Lagrangian- Eulerian Approach to Modeling Homogeneous Condensation in High Density Gas Expansions (Postprint)				5a. CONTRACT NUMBER	
				5b. GRANT NUMBER	
				5c. PROGRAM ELEMENT NUMBER	
6. AUTHOR(S) Ryan Jansen (USC); Natalia Gimelshein and Sergey Gimelshein (ERC), and Ingrid Wysong (AFRL/RZSA)				5d. PROJECT NUMBER	
				5f. WORK UNIT NUMBER 23080532	
7. PERFORMING ORGANIZATION NAME(S) AND ADDRESS(ES) University of Southern California University Park Los Angeles, CA 90089				8. PERFORMING ORGANIZATION REPORT NUMBER	
9. SPONSORING / MONITORING AGENCY NAME(S) AND ADDRESS(ES) Air Force Research Laboratory (AFMC) AFRL/RZS 5 Pollux Drive Edwards AFB CA 93524-7048				10. SPONSOR/MONITOR'S ACRONYM(S)	
				11. SPONSOR/MONITOR'S NUMBER(S) AFRL-RZ-ED-JA-2010-526	
12. DISTRIBUTION / AVAILABILITY STATEMENT Approved for public release; distribution unlimited (PA #10630).					
13. SUPPLEMENTARY NOTES Published in the AIP Journal of Chemical Physics: J. Chem. Phys. 134 , 104105 (2011) ©American Institute of Physics					
14. ABSTRACT A computational approach to homogeneous nucleation is proposed based on Eulerian description of the gas phase expansion coupled with a Lagrangian approach to the cluster formation. A continuum, Euler/Navier–Stokes solver versatile advection code is used to model the gas transport, and a kinetic particle solver is developed in this work to simulate cluster nucleation and growth. Parameters in the new model were adjusted so as to match the known theoretical dimer formation equilibrium constants for the two gases under consideration, argon and water. Reasonable agreement between computed and available experimental data was found in terminal cluster size distributions for nozzle water expansions in a wide range of stagnation pressures. The proposed approach was found to be orders of magnitude faster than a comparable approach based on the direct simulation Monte Carlo method.					
15. SUBJECT TERMS					
16. SECURITY CLASSIFICATION OF:			17. LIMITATION OF ABSTRACT	18. NUMBER OF PAGES	19a. NAME OF RESPONSIBLE PERSON
a. REPORT	b. ABSTRACT	c. THIS PAGE			Dr. Ingrid Wysong
Unclassified	Unclassified	Unclassified	SAR	13	19b. TELEPHONE NUMBER <i>(include area code)</i> N/A

A Lagrangian–Eulerian approach to modeling homogeneous condensation in high density gas expansions

Ryan Jansen, Natalia Gimelshein, Sergey Gimelshein, and Ingrid Wysong

Citation: *J. Chem. Phys.* **134**, 104105 (2011); doi: 10.1063/1.3562370

View online: <http://dx.doi.org/10.1063/1.3562370>

View Table of Contents: <http://jcp.aip.org/resource/1/JCPSA6/v134/i10>

Published by the [American Institute of Physics](#).

Additional information on *J. Chem. Phys.*

Journal Homepage: <http://jcp.aip.org/>

Journal Information: http://jcp.aip.org/about/about_the_journal

Top downloads: http://jcp.aip.org/features/most_downloaded

Information for Authors: <http://jcp.aip.org/authors>

ADVERTISEMENT

**AIP**Advances

Submit Now

**Explore AIP's new
open-access journal**

- **Article-level metrics
now available**
- **Join the conversation!
Rate & comment on articles**

A Lagrangian–Eulerian approach to modeling homogeneous condensation in high density gas expansions

Ryan Jansen,¹ Natalia Gimelshein,² Sergey Gimelshein,^{2,a)} and Ingrid Wysong³

¹University of Southern California, Los Angeles, California 90089, USA

²ERC, Inc., Edwards AFB, California 93524, USA

³Air Force Research Laboratory, Edwards AFB, California 93524, USA

(Received 7 December 2010; accepted 14 February 2011; published online 9 March 2011)

A computational approach to homogeneous nucleation is proposed based on Eulerian description of the gas phase expansion coupled with a Lagrangian approach to the cluster formation. A continuum, Euler/Navier–Stokes solver versatile advection code is used to model the gas transport, and a kinetic particle solver is developed in this work to simulate cluster nucleation and growth. Parameters in the new model were adjusted so as to match the known theoretical dimer formation equilibrium constants for the two gases under consideration, argon and water. Reasonable agreement between computed and available experimental data was found in terminal cluster size distributions for nozzle water expansions in a wide range of stagnation pressures. The proposed approach was found to be orders of magnitude faster than a comparable approach based on the direct simulation Monte Carlo method. © 2011 American Institute of Physics. [doi:10.1063/1.3562370]

I. INTRODUCTION

Homogeneous condensation plays an important role in many atmospheric and technological processes, and understanding its physical mechanisms and dependencies is critical for a number of engineering applications. One such application, pertaining to post boost vehicle operations at very high altitudes, is related to thruster plume expansion into the surrounding rarefied atmosphere.¹ It is well known that particulates of different kinds are the main contributor to the scattering of sunlight observed in high altitude plumes. The effect of sunlight scattering in plumes in which neither carbon soot nor alumina particles were present in significant concentrations, with the specific example of the Apollo 8 translunar injection burn,² indicates that particles must be formed in the rapid expansion of the exhaust to the rarefied atmosphere, mostly from the condensation of water vapor and other combustion products in the plume.

Condensation in rapidly expanding flows has been observed experimentally as early as the mid-1930s (Ref. 3) and has been extensively studied in the following decades (see for example Ref. 4 and the references therein). Computational modeling of expanding condensing flows has a shorter, although still a respectable history. In the past, two different approaches have been used to describe homogeneous condensation and, in particular, cluster nucleation (formation of small clusters from monomers) in the nonequilibrium environment of rapid expansions. In the first approach, based on the classical nucleation theory (CNT) (Ref. 5) and equilibrium thermodynamics, the key process is the formation of the smallest stable droplets possible, so-called critical clusters, through unimolecular reactions of cluster growth and decay. The classical theory calculates the condensation and evaporation rates using the Gibbs distributions and the

principle of detailed balance, and the nucleation rate is then calculated assuming a steady state condition.⁶

The main principles of the classical nucleation theory in combination with the conventional compressible Euler or Navier–Stokes gas dynamic equations were used by a number of researchers to predict numerically multidimensional condensing flows (see, for example, Refs. 7–9). The important part of these models is the creation of cluster nuclei at some critical size that depends on local gas conditions. The nucleation rate is governed by CNT and droplet growth can be derived on the basis of heat transfer conditions surrounding the droplet (the description of Ref. 10 was used in Ref. 8). Both Eulerian⁷ and Lagrangian⁸ descriptions of condensed droplets have been used in the literature.

An alternative approach to modeling homogeneous condensation is based on some assumed shape of the droplet size distribution, usually lognormal. In Ref. 11, this assumption is coupled with a modified form of the Hertz–Knudsen equation, which gives the droplet–gas mass transfer rate as the difference between incoming fluxes from the gas phase and evaporative fluxes from the droplet; a standard Eulerian description was used to model the two-phase flow. In Ref. 12, viscous compressible reduced Navier–Stokes equations¹³ are used for the gas phase, while the polydisperse particle behavior is described by the Eulerian aerosol moment model which accounts for particle transport due to convection, diffusion, inertia, and thermophoresis, as well as particle dynamics due to coagulation, nucleation, and condensation. Yet another numerical approach, which uses many of the CNT assumptions and has been applied mostly to turbulent condensing flows, is based on a semi-Lagrangian treatment of droplets.^{14,15} Semi-Lagrangian methods combine both Eulerian and Lagrangian points of view: a scalar field is discretized on the Eulerian grid but is advanced in time using a Lagrangian technique.

While different methods were applied to predict cluster nucleation and growth in gas flows, most of the researchers

^{a)}Electronic mail: gimelshe@usc.edu.

that used the classical nucleation theory applied the Eulerian approach to the gaseous phase, usually based on the solution of full or reduced Navier–Stokes equations. A different strategy was proposed in Ref. 16, where a particle-based direct simulation Monte Carlo (DSMC) method¹⁷ was used to compute the gas flow. A Lagrangian technique was applied to model cluster evolution. Similar to Ref. 7, new clusters were created at a critical size, and their further growth was calculated with the CNT approach.

Some important assumptions of the CNT, such as unimolecular reactions of cluster growth and decay, and the use of the principle of detailed balance that implies thermodynamic equilibrium, limit its applicability as a prediction tool for highly nonequilibrium flows, such as rapidly expanding plumes. In such flows, the impact of thermal nonequilibrium between gas and particles is expected to significantly impact the growth rates and cluster size distributions. Moreover, the cluster size distribution may have a significantly more complex shape than the lognormal distribution often used in the literature. An illustrative example of such complex distributions was provided in Ref. 18, where the terminal cluster size distributions were measured in water and ammonia expansions for a wide range of stagnation pressures and temperatures; the results were obtained by doping the water and ammonia clusters by one Na atom, which was photoionized close to the threshold without fragmentation.

The experimental study¹⁸ showed that, for lower pressures, the size distribution is exponential; for higher pressures, the size distribution approaches the lognormal profile, and, for intermediate pressures, it has a complex bimodal shape. The transition from the exponential to the bimodal shape was explained by changing governing mechanisms of cluster growth. For lower pressures, the clusters grow mostly through monomer sticking, while at higher pressures, the main mechanism is cluster–cluster collisions and coalescence. The bimodal shape of the cluster size distribution function for intermediate plenum pressures was attributed in Ref. 18 to the coalescence of small particles (such as dimers and trimers) on larger clusters and the coagulation of larger clusters. A bimodal distribution of cluster sizes was measured¹⁸ for a number of chamber pressures, varied by up to an order of magnitude; typically, it was observed when the average cluster size was from below 100 to about 1000. These cluster sizes are believed to be largely occurring in a number of applications, including rocket thruster plumes.

The inability of CNT-based methods to accurately predict the cluster size distributions in strongly nonequilibrium flows dictates the use of the second approach, known as the kinetic approach, which treats nucleation as the process of kinetic chemical aggregation.¹⁹ Unlike CNT, the kinetic approach does not assume local thermodynamic equilibrium. Instead, a microscopic process of the interactions of monomers and clusters is described either analytically via a mathematical model, e.g., by the Smoluchowski equations where the interaction between particles is modeled by the reaction rates,^{20,21} or in computer simulations, e.g., in molecular dynamics (MD) calculations where the interaction is modeled by an interaction potential.^{22,23} It is well known that the application of either the Smoluchowski equations or the molecular dynamics

approach to the modeling of cluster evolution in multidimensional thruster plume flows is computationally unfeasible.

A more promising direction in modeling rapidly expanding condensing flows is the use of the DSMC method. As a numerical approach to the Boltzmann equation, it is applicable to a large range of flow conditions. In this method, cluster–cluster and cluster–monomer interactions including the multibody reactions of cluster nucleation can be seamlessly incorporated. Over the last several years, the DSMC method has been extensively and successfully applied to modeling cluster formation and evolution in supersonic jets.^{24,25} The work of these authors²⁶ extended the kinetic dimer formation approach of Ref. 27, which assumed that a ternary collision always results in a dimer formation, to include MD simulations for obtaining information on the probability of dimer formation in such ternary collisions. The work²⁸ used a temperature-dependent probability of formation of argon dimers. Another DSMC-based model, which treats both cluster nucleation and evaporation [Rice, Ramsperger, and Kassel, or RRK (Ref. 29) technique was used for the latter] from the principles of the kinetic theory, was introduced in Ref. 30.

The difficulty of using the DSMC method as the modeling approach for condensing plumes is its high computational cost. It may be applied to relatively low density plumes, when the typical size of clusters does not exceed 100-mers. For higher pressures, this approach becomes prohibitively expensive. The most serious numerical limitation of the DSMC method is related to the fact that a large number of simulated particles has to be computed. The required number of simulated particles generally increases as n^2 for 2D problems, and n^3 for 3D problems, where n is the gas density. Most of the simulated particles are monomers; the statistical scatter for cluster species is, therefore, extremely high as compared to the monomers. The use of species weights in the DSMC method is questionable, since clusters, especially for larger pressures, are not a trace species, and thus strongly impact the flow properties through the heat release during the nucleation and cluster growth process.

The main objective of this work is the development of a new method that would combine the computational efficiency of the Eulerian continuum approach and the physical accuracy of the Lagrangian kinetic approach. The proposed method integrates the Eulerian approach for monomer gas flow based on the solution of Euler/Navier–Stokes equations, with the Lagrangian approach for cluster formation and evolution based on a DSMC-like particle-based algorithm. The work is built on the previous effort³⁰ where the first-principles model of homogeneous condensation was formulated, and all of the most important processes of cluster nucleation and evolution were considered at the microscopic level. The processes included in the model³⁰ are (i) creation of dimers through the collision stabilization of collision complexes, (ii) elastic monomer–cluster collisions that change the translational and internal energies of colliding particles, (iii) inelastic monomer–cluster collisions that result in monomer sticking, (iv) cluster–cluster coalescence, and (v) evaporation of monomers from clusters. All these processes are present in the new method. In Sec. II, the details of the method are discussed, and the

homogeneous nucleation rates in argon and water thermal bath environments are analyzed, followed by the validation study that focuses on comparison of cluster growth in plumes with available experimental data on terminal cluster size distribution.

II. NUMERICAL APPROACH

The main idea of the present numerical method is to calculate gas flow solving the compressible Euler or Navier–Stokes equation, model the nucleation process starting from the dimer formation and up using the elementary kinetic theory for cluster–cluster and cluster–monomer collisions, and exchange the information between the continuum and kinetic parts of the simulation through source terms, so that these parts are fully coupled. Similar to the DSMC method, a finite number of simulated clusters replace the real ones, so that each simulated cluster represents a large number of real particles. The obvious benefit of this approach is related to the combination of the numerical efficiency of computing the carrier gas flow with a continuum Eulerian method and physical accuracy of modeling the cluster evolution with a kinetic theory based technique.

A. Eulerian approach to gas phase expansion

The Eulerian–Lagrangian approach with a two-way coupling developed in Ref. 31 to model two-phase plume flows represents the computational framework of the new condensation model. The gas flow is computed using the Eulerian approach based on the solution of the Euler equations with appropriate source terms that take into account the impact of condensation process and clusters on the gas flow:

$$\frac{\partial \rho}{\partial t} + \nabla \cdot \rho \mathbf{v} = M, \quad (1)$$

$$\frac{\partial \rho \mathbf{v}}{\partial t} + \nabla \cdot \rho \mathbf{v} \mathbf{v} + \nabla p = D, \quad (2)$$

$$\frac{\partial e}{\partial t} + \nabla \cdot (e + p) \mathbf{v} = Q, \quad (3)$$

where M , D , and Q are the corresponding mass, momentum, and energy source terms that define the impact of condensation on gas molecules, and ρ , \mathbf{v} , p , and e are the gas density, velocity, pressure, and energy, respectively.

The Euler equations are solved using the versatile advection code (VAC) (Ref. 32) modified to include the above source terms. Particle properties are determined by Lagrangian tracking of particles through the gas flowfield and statistical averaging of particle parameters. For the gas phase, an explicit time integration is used, and the gas dynamic equations are solved using the total variation diminishing (TVD)-Lax–Friedrichs scheme with minmod limiter. For the particle phase, a fourth order Adams–Moulton method is used to integrate particle equations of motion.

In the current implementation, the clusters are assumed to be in translational equilibrium with the gas, that is, their

macroscopic velocity and translational temperature are assumed to be equal to the corresponding parameters of the gas. This significantly simplifies the implementation, since then there is no need for the calculation of cluster drag. At the same time it results in an approximate treatment of the gas–cluster heat and momentum transfer, since the drag component is not included in the heat transfer process. Note that since the clusters are small, the drag contribution to the heat transfer is expected to be noticeably smaller than that coming from the temperature difference. Note also that a more accurate model could be developed that would take into account the separation between cluster and gas velocities and the drag force from gas to droplets, as well as viscous terms in the gas phase equations. However, it is out of the scope of this work, where the primary scope is the introduction of a new particle-based condensation model capable of a two-way coupling with a continuum solver.

At each time step Δt , the clusters are moved by $\mathbf{v}_i \Delta t$, where \mathbf{v}_i is the velocity of the i th cluster. Then, the cluster collision relaxation processes are modeled at the kinetic level. These processes, that include the formation of new dimers, monomer–cluster collisions that involve energy transfer between internal and translational modes of colliders, cluster–cluster coalescence, and cluster growth and shrinking due to monomer sticking and evaporation, are described in detail below. After the cluster relaxation processes, the changes in cluster mass and internal energy are evaluated, and then used to calculate the right-hand side of the Navier–Stokes equations.

B. Lagrangian approach to cluster formation and evolution

Replacing the kinetic modeling of gas transport with a continuum approach is justified by the proximity to equilibrium of velocity distribution functions of gas molecules in condensing plumes, where the gas density is fairly large, and the mean free path is many orders of magnitude smaller than the characteristic flow size (usually nozzle throat or exit diameter). The cluster nucleation and evaporation processes, though, require kinetic treatment for a number of reasons, most notably nonequilibrium cluster size distribution and the departure from equilibrium of cluster internal energies. Such a kinetic, Lagrangian treatment is, therefore, proposed in the present work. Although the kinetic, Lagrangian approach to modeling cluster nucleation follows to some extent the first principle, fully kinetic approach of the previous work,³⁰ it has a number of key differences, mostly related to the fact that monomers are simulated at the continuum level. Thus, some approximation has to be used to include cluster-related collisions that involve monomers.

1. Dimer formation

Dimers are formed as a result of a collisional stabilization of collision complexes consisting of two monomers that collide with third particles during their lifetime; the third particle is needed to carry away extra energy and,

thus, stabilize the dimer. In each stabilization event, there is also an energy release from the intermolecular potential of the two monomers that formed the collision complex into the internal energy modes of the newly created dimer and the third particle, and the translational modes of their relative motion.

The change in the dimer number density Δn_d as a result of new dimers formed in each cell over a single time step Δt is calculated from the known recombination rate and macroscopic gas properties in the cell as follows:

$$\Delta n_d = K_{\text{rec}} n^3 \Delta t. \quad (4)$$

Here, K_{rec} is the recombination rate constant and n is the gas number density. Then, the number of newly created dimers is given by $\Delta n_d V_c / F_{\text{num}}$, where F_{num} is the number of real clusters represented by one simulated cluster (similar to F_{num} traditionally used in the DSMC method) and V_c is the cell volume. Generally, any form of temperature dependence may be used to define K_{rec} ; in this work, a temperature dependence similar to the well known Arrhenius dependence is used, $K_{\text{rec}}(T) = A \times B^T \exp(-CT)$. In this equation, constants A , B , and C may be chosen either from values known in the literature or selected to reproduce analytical dimer formation equilibrium constants. Note that the reverse process of dimer loss is not shown in Eq. (4) since it is included separately through collisional and evaporative mechanisms discussed in Secs. II B 3–II B 4.

The initial position of each formed dimer is selected randomly within the cell, its initial velocity is set equal to the macroscopic velocity of the gas in the cell, and the initial cluster internal energy is sampled as follows. First, the total available energy in the collision complex-third particle collision is assumed to be equal to

$$E_{\text{tot}} = \left(\frac{3}{2} \xi_{\text{int},1} + \frac{4 - 2\alpha_m}{2} + \frac{4 - 2\alpha_c}{2} \right) kT, \quad (5)$$

where ξ_{int} is the number of internal degrees of freedom of the monomer (zero if atom), k is the Boltzmann constant, and α is the variable hard sphere (VHS) model¹⁷ parameter. Although a more sophisticated model of the intermolecular potential may be used here, the VHS model is chosen as a simple potential that was proved to be accurate and efficient on kinetic modeling of plume flows. In this work, standard VHS values for argon¹⁷ were used, $\alpha_m = \alpha_c = 0.31$. For water, the values $\alpha_m = \alpha_c = 0.5$ were chosen that provide a reasonable approximation of the viscosity-temperature dependence in the range of temperatures of interest.

In Eq. (5), the $4 - 2\alpha_m$ term corresponds to the number of relative translational degrees of freedom in the monomer–monomer collision, and $4 - 2\alpha_c$ is the number of relative translational degrees of freedom in the interaction of a collision complex and a monomer. After that, the total energy is increased by evaporation (dimer dissociation) energy E_{evap} and then split between the newly created dimer and the third particle using the Larsen–Borgnakke (LB) (Ref. 33) procedure. This procedure, initially developed to model energy transfer between translational and rotational modes of colliding molecules, is based on the assumption that

after-collision relative translational and internal energy modes will be populated according to the local equilibrium distribution functions.

In this work, the energy transfer was assumed to include all available after-collision energy modes, i.e., energy of relative motion of the dimer–monomer pair, the internal energy of the monomer, and the internal energy of the dimer. The energy $E_{\text{tot}} + E_{\text{evap}}$ is, thus, split between those modes using the LB approach. For monomers, only rotational modes are assumed to be excited, since at low gas temperatures in expanding plumes (below 300 K in this work) the excitation of vibrational modes is negligible. The number of internal degrees of freedom of the dimer is calculated from the dimer heat capacity C_v using a general expression

$$\xi^{\text{int},i} = i \frac{2C_v}{k} - 3, \quad (6)$$

where i is the number of monomers in the clusters ($i = 2$ for dimer). Note that this expression is also utilized for larger clusters. The values of heat capacities used in this work for argon and water clusters are taken from Ref. 30 and are highly uncertain.

The dimer formation procedure, thus, results in the formation of dimers at a given temperature-dependent rate, and each of these dimers is characterized by a unique internal energy that is subsequently used in the cluster collision and evaporation processes.

2. Inelastic monomer–cluster collisions

The interaction between monomers and clusters is an important process that results in energy transfer between the internal modes of clusters and translational modes of colliders. The change in the cluster internal energies has a great impact on the evaporation rates and, thus, needs to be modeled properly. It was pointed out in Ref. 30 that when the LB model is used to simulate the energy transfer in monomer–cluster collisions, it is reasonable to introduce an inelastic collision relaxation number Z , which defines the probability P_{inel} that a cluster will experience an inelastic collision leading to a change in its internal energy in a single collision as $P_{\text{inel}} = 1/Z$. This means that in the model, only one out of every Z collisions of a cluster will change its internal energy, and all other collisions will be elastic. In every collision that involves such a change, the after-collision energies are selected according to the local equilibrium distribution functions. This is a simplification of the actual process, where internal energy change may occur in every collision. It is also similar to the rotational and vibrational relaxation numbers Z_r and Z_v widely used in the DSMC method. Values of Z were proposed in Ref. 30 that provide good agreement with known theoretical dimer formation equilibrium constants for argon and water; these values are used in this work. For water, $Z = 10$ over all temperatures, and for argon, it depends on gas temperature T , increasing from 3 at $T \approx 0$ to 25 at $T = 500$ K.

A similar approach is used in the present model, with one significant exception. Among many monomer–cluster collisions, only those that cause the cluster internal energy change

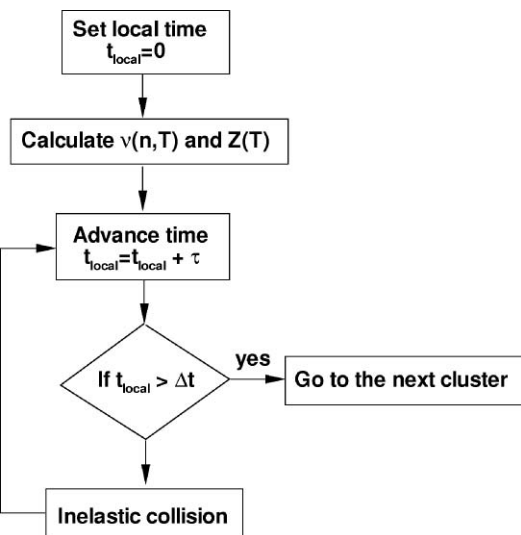


FIG. 1. Flow chart for cluster–monomer inelastic collision modeling.

are important in terms of cluster evolution, and, thus, only those collisions were modeled. Since the value of Z is typically noticeably larger than one, such an approach allows for significant reduction in computational time. The algorithm, therefore, is reduced to the analysis of each cluster in the computational domain in terms of possible inelastic collisions with monomers as follows.

First, note that the probability that a cluster will experience an inelastic collision leading to a change in its internal energy during time τ is equal to $p = 1 - \exp(-\nu\tau/Z)$, where ν is the collision frequency of clusters on monomers. Therefore, the time to the next inelastic collision can be sampled as $\tau_{\text{next}} = -Z/\nu \log(\mathfrak{R})$, where \mathfrak{R} is the random number uniformly distributed between 0 and 1. The algorithm to model inelastic collisions for a given cluster over time step Δt is given in Fig. 1.

Unlike Ref. 30, where the kinetic, microscopic information on monomers that include their individual energy states and velocities is available, the present method provides only the macroscopic information such as temperature and number density. While sufficient to calculate the local collision frequency and temperature-dependent internal energy relaxation number Z , this is not enough to simulate monomer–cluster collisions at the kinetic level. In order to do that, additional information about the velocity and energy distribution functions of monomers is necessary. In this work, the internal energy of the colliding monomer and the relative translational energy of the colliding monomer–cluster pair are sampled from the corresponding equilibrium distributions. Note that it is also possible to use the Chapman–Enskog distribution function³⁴ for the translational modes, but the results in most situations are not expected to be significantly different. The total collisional energy, which is the sum of these two energies and internal energy of the cluster, is then redistributed between the relative translational and the internal modes of the cluster and the monomer using the LB model. The numbers of the corresponding degrees of freedom are defined as described in the dimer formation section.

3. Cluster growth and evaporation

The key processes that determine small cluster evolution are sticking and evaporation of monomers off the clusters. In order to drastically reduce the requirements to the minimum time step used in the simulation and provide an accurate account of the evaporation, and sticking events of a single cluster, the growth and evaporation processes are combined in a single procedure as follows.

The cluster sticking rate is calculated as $\nu_s = nP_s\langle\sigma_c g\rangle$, where P_s is the probability that a monomer will stick to the cluster after the collision, σ_c is the monomer–cluster collision cross section (in this work it is calculated using the hard sphere model) and g is the relative collision velocity. In the hard sphere model, where the collision cross section is written as πd^2 , the collision diameter d is given as the average of the diameter of the colliding monomer obtained from the VHS model¹⁷ (4.17 Å for argon and 6.2 Å for water) and the cluster diameter obtained through an empirical correlation used extensively in the past (see, for example, Ref. 16):

$$d_c = 2 \times (A \cdot i^{1/3} + B), \quad (7)$$

where A and B are species-dependent constants. In this work, the values of A and B were 2.3×10^{-10} and 3.4×10^{-10} m for argon,²⁴ and 1.9×10^{-10} and 2.4×10^{-10} m for water.³⁵

For the water monomer–cluster sticking collision probability, the empirical dependence of the probability, ϵ on the species diameter d and mass m given in Ref. 36 is used. After a simple transformation, one may write

$$\epsilon = \frac{d_i^2}{(d_i + d_1)^2} \left(\frac{m_i}{m_i + m_1} \right)^{1/2}, \quad (8)$$

where indices i and 1 refer to the cluster of size i and the monomer, respectively. For argon monomer sticking, the size dependent probability of Ref. 30 is used, where the sticking probability increases with cluster size, from 0.06 for monomer–dimer collisions to 0.9 for monomer–15-mers collisions.

To evaluate the rate of evaporation of monomers from the cluster surface, the RRK model²⁹ is used, similar to Ref. 30. Following Ref. 37, this work calculates the evaporation rate k_e using

$$k_e = \nu N_s \left(\frac{E_{\text{int}} - E_{\text{evap}}}{E_{\text{int}}} \right)^{3i-7}. \quad (9)$$

Here, ν is the vibration frequency, N_s is the number of surface atoms, and E_{int} is the cluster internal energy. For dimers, the exponent $3i - 7$ is replaced with 1. The number of surface atoms N_s is i for $i < 5$, $i - 1$ for $4 < i < 7$, and $(36\pi)^{1/3}(i^{1/3} - 1)^2$ for $i > 6$. The vibration frequency was taken to be 10^{12} s^{-1} for argon clusters³⁷ and $2.68 \times 10^{12} \text{ s}^{-1}$ for water clusters.³⁸

With the evaporation and sticking rates defined by the above expressions, the algorithm used to model sticking and evaporation processes is given in Fig. 2. For cluster growth (monomer sticking), the monomer internal energy and relative translational energy are sampled from the corresponding equilibrium distributions, and the after-sticking cluster internal energy is equated to the sum of cluster precollisional

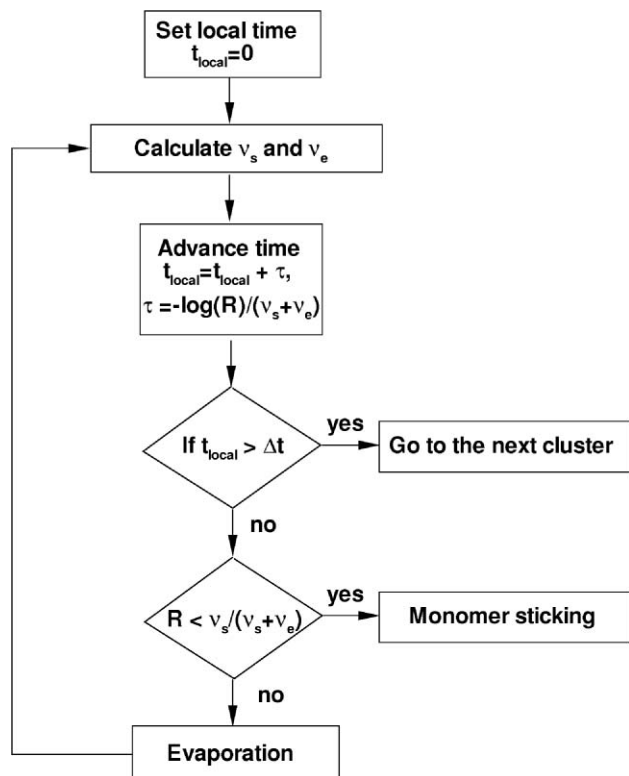


FIG. 2. Flow chart for cluster growth and evaporation modeling.

internal energy, internal energy of the monomer, relative translational energy, and evaporation energy E_{evap} .

For cluster evaporation, the cluster internal energy is decreased by E_{evap} , and the remaining energy is redistributed between the cluster internal modes, internal modes of the departing monomer, and relative translational modes using the LB model. Note here that only the cluster internal energy is calculated, while the cluster velocity and monomer properties are assumed to accommodate to the gas properties.

4. Cluster–cluster collisions

The cluster–cluster collisions must be taken into account for an accurate description of cluster evolution, since it is the key factor determining the size distribution of larger clusters. Cluster–cluster collisions have different outcomes, which generally may be classified as either coalescence or reflexive and stretching separations. The dynamics of water droplet collisions for macroscopic particles was studied experimentally in Ref. 39 where the boundaries between both of the separating collisions and the coalescence collision were examined as a function of the size ratio and the Weber number in the wide range of Weber numbers from 1 to 100. For microscopic particles with sizes from dimers to 1000-mers, the authors are not aware of any comparable to the Ref. 39 systematic study where the results of cluster collisions would be analyzed for different Weber numbers. Extrapolating the results of Ref. 39 to microscopic particles of interest in this work, one can notice that for typical plume temperatures on the order of 100 K and, thus, Weber numbers on the order of the unity or less, the clusters would mostly experience coa-

lescence and not separation. However, such an extrapolation, although partially justified for 100-mers and 1000-mers, is much more questionable for smaller clusters, where more reflexive collisions may be expected. In this work, in the absence of reliable size and relative velocity dependence of the collision outcome for small clusters, a constant coalescence probability is assumed.

The cluster–cluster collisions are modeled using the conventional DSMC algorithm. The majorant frequency scheme⁴⁰ of the DSMC method was utilized for this purpose. At every time step, the maximum cluster size is obtained in each cell. Then, the majorant collision frequency is calculated based on this maximum cluster size and maximum relative collision velocity evaluated from the local gas temperature. The majorant collision frequency is then multiplied by the coalescence probability, since only the coalescence events are modeled (reflexive separation is believed to have negligible effect on cluster properties, and the stretching separation process is not included in the present model). After a pair of clusters K and L is selected for physical collision, the coalescence event is modeled, with the result being a larger cluster M with mass m and internal energy E_{int} calculated from the properties of colliding clusters using the mass and energy conservation constraints. The laws dictated

$$m_M = m_K + m_L, \quad E_{\text{int},M} = E_{\text{int},K} + E_{\text{int},L} - Q,$$

with $Q = -Q_M + Q_K + Q_L$, where Q_i is the energy of vaporization of cluster i .

After all collision and evaporation processes are simulated for a given time step, the mass and energy changes over this time step are calculated over all cells in order to be included in the Eulerian gas flow equations. The primary purpose of this step is accurate conservation of all conservative properties in the simulation.

III. THERMAL BATH RELAXATION

Inelastic cross sections for monomer–monomer and monomer–cluster collisions are needed as part of a comprehensive validation of a kinetic condensation model. These cross sections, in general a function of the translational and internal energy states of precollision and postcollision particles, are unavailable for the species and temperatures desired. However, equilibrium rates for nucleation and evaporation for both water and argon are available in literature. Furthermore, a necessary condition for the model to fulfill is that it produces correct behavior in equilibrium, although it does not guarantee the model will have correct nonequilibrium behavior.

Such equilibrium behavior was modeled in this work by a thermal bath relaxation of both argon and water at various temperature conditions. The equilibrium constants for the formation of clusters were calculated and compared to published results of Refs. 41–43. In addition, they were compared to the previously obtained results of the DSMC-based model.³⁰

To model argon equilibrium, over 1×10^6 simulated particles were used, and the run was allowed to run until a steady equilibrium value was reached, usually about half a million time steps. The time step for argon was selected to be

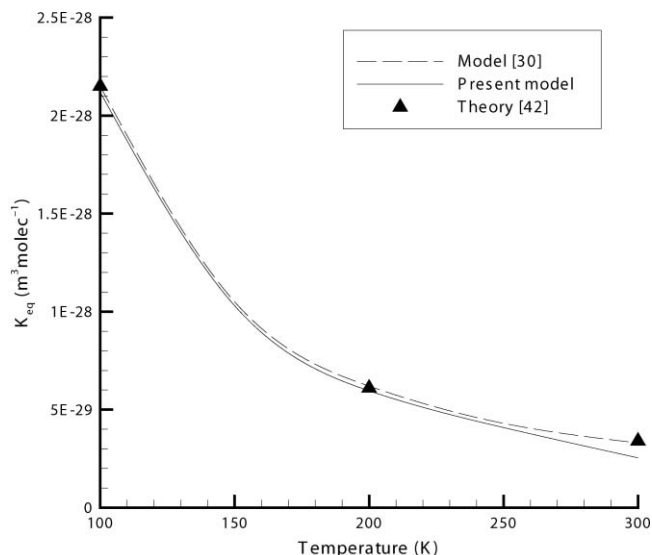


FIG. 3. Argon dimer formation equilibrium constant as a function of gas temperature.

10^{-10} s, so that there was on average fewer than one collision per molecule per time step, making the results independent of step size. A monomer number density of 10^{22} molecules/ m^3 was selected to ensure that clusters made up less than 0.1% of the gas while maintaining the 10×10^6 particle requirement. This ensured that adequate numbers of particles were present for statistics, and that the clusters did not have a significant impact on the behavior of the gas.

The dimer formation rate k_{rec} for argon was computed using the stable dimer formation rate from Ref. 41, which is written as

$$k_{\text{rec}} = A \times B^T \exp(-CT). \quad (10)$$

The values of A , B , and C given in Ref. 41 are $A = 10.15 \times 10^{-44} \text{ m}^6 \text{ molecules}^{-2} \text{ s}^{-1}$, $B = -0.278$ and $C = 3.10 \times 10^{-3} \text{ K}^{-1}$.

The argon equilibrium constant as a function of temperature is shown in Fig. 3. It is compared with the DSMC results from Ref. 30 and the theoretical predictions of Ref. 42. There is good agreement between this model and the theoretical predictions, although it becomes somewhat worse at higher temperatures. Since the condensation of argon is very small at those temperatures, such a deviation is not expected to matter in plume flows. Note also that the present model uses the values of the inelastic collision number Z as a function of temperature taken from Ref. 42, where this parameter was adjusted to fit the equilibrium constant of Ref. 42 in the range of temperatures between 100 and 300 K. No fitting of any numerical or physical parameter of the present model to match the theoretical equilibrium constants was conducted for argon, which resulted in some difference.

In modeling water equilibrium, about 1×10^6 simulated particles were used, and the process was again allowed to run until a steady equilibrium was reached, about half a million time steps. The time step was set at 1×10^{-8} s, which ensured not only that there was still much fewer than one collision per particle per time step, but also that the system

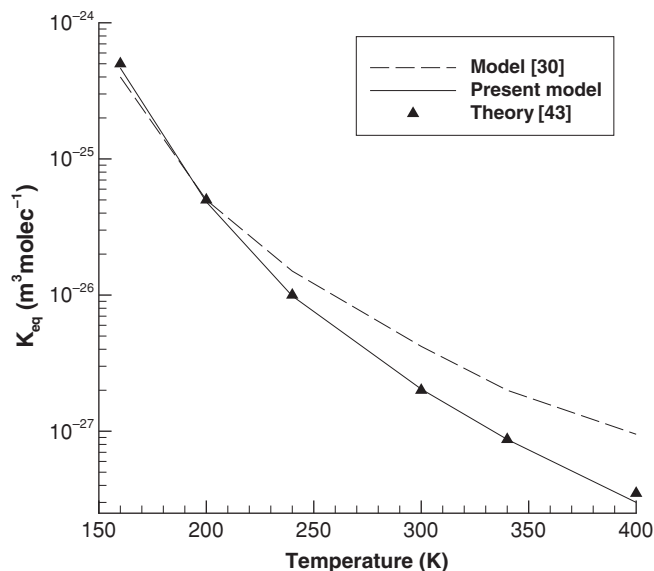


FIG. 4. Water dimer formation equilibrium constant as a function of gas temperature.

would reach complete equilibrium within a reasonable number of time steps. A number density of 10^{21} molecules/ m^3 was selected to ensure that clusters were less than 0.1% of the gas while maintaining 1×10^6 simulated particles. Due to the low fraction of clusters, this ensured that the behavior of the gas was not influenced by the presence of the clusters. Note that using a smaller gas density does not change the results of the simulations.

The authors are not aware of any theoretical, experimental, or computational results that would provide the temperature-dependent rate of dimer formation, similar to that of Ref. 41 for argon. Although it is generally possible to use a rate obtained from the kinetic theory for binary and ternary collisions, such a rate would inherently include a number of assumptions and adjustable parameters, such as the dimer stabilization probability, the collision complex lifetime, and others, that would affect the obtained equilibrium constant. It appears more reasonable, therefore, to use a dimer formation rate that provides acceptable agreement with available dimer formation equilibrium constants. In this work, the Arrhenius expression given by Eq. (10) was used, with constants adjusted to produce the given equilibrium constants: A , B , and C are found to be $A = 5.42 \times 10^{-41} \text{ m}^6 \text{ molecules}^{-2} \text{ s}^{-1}$, -1 , and $2.2 \times 10^{-3} \text{ K}^{-1}$.

The water equilibrium constant is shown in Fig. 4. It is compared with the theoretical predictions⁴³ and the numerical results of the DSMC-based model.³⁰ As expected from using adjusted constants in Eq. (10), there is excellent good agreement between the current model and the results of Ref. 43 at all temperatures investigated in this work. Furthermore, the present model provides a much better ability to match dimer formation equilibrium constants than Ref. 30.

IV. WATER CLUSTER SIZE DISTRIBUTION IN NOZZLE EXPANSION

The second part of the validation and numerical analysis of the presented condensation model is focused on the

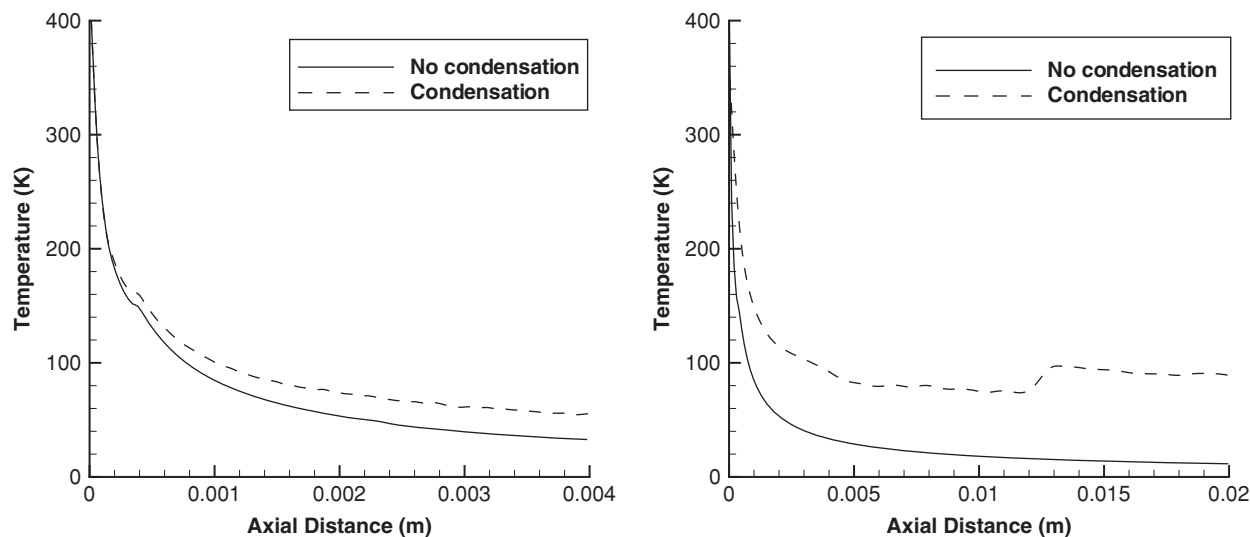


FIG. 5. Gas temperature profile along the nozzle axis for $p_0 = 1.577$ bars (left) and $p_0 = 8.307$ bars (right).

nucleation and evolution of small water clusters in a conical nozzle. The study was prompted by the availability of high quality experimental data¹⁸ on the terminal size distribution of water clusters in the wide range of flow conditions where the cluster size distribution changes its shape from exponential at low pressures to bimodal at intermediate pressure to lognormal at high pressures. The experimental results were obtained by doping the water clusters by one Na atom, which is photoionized close to the threshold without fragmentation. The nozzle has a conical diverging section with a 41° opening angle, a total length of 2 mm, and a throat diameter of $50 \mu\text{m}$. Four different stagnation pressures were computed, considered in Ref. 18, 1.577, 2.173, 5.144, and 8.307 bars, with the corresponding stagnation temperature of 495 K. Since the background pressure effect in the experiment is believed to be small,⁴⁴ expansion into a vacuum is modeled.

The computations were conducted on a 500×150 spatial grid, with cell sized reduced in the radial direction and increased in the axial direction. Previous studies³⁰ have shown an insignificant impact of the wall conditions on the coreflow where the cluster sizes are recorded, so that the use of the Euler solver for the gas phase is reasonable. The number of simulated droplets was about 500 000, which was found to provide adequate statistical accuracy for the calculations. The particles were assumed to condense on the nozzle surface. Uniform inflow conditions were imposed at the nozzle throat, calculated from the isentropic flow relations. To compare the cluster size distributions with the terminal distributions¹⁸ measured far downstream from the nozzle, the computed size distributions at several stations along the nozzle axis were analyzed to provide truly terminal, distance-independent distributions. The domain size was increased in the axial direction from 4 mm for the lowest pressure to 20 mm for the highest pressure to ensure that the size distributions at the exit boundary are essentially frozen.

A typical run time for the lowest pressure under consideration was several hours and for the highest pressure was up to 2 days on a single processor computer. Comparing these numbers with those of Ref. 30 where a DSMC method was

used to model a 1.577 bars water expansion, one finds that the new approach is about 50 times faster than the DSMC-based method for the lowest pressure. This factor will grow significantly with pressure. The reduction in run time is mostly related to the time efficient modeling of gas transport with a continuum method. Since clusters comprise only a relatively small fraction of the particles in the flow, gas transport modeling is the most time consuming part of any DSMC-based technique. Note that species weights for cluster species would reduce the time requirements of the DSMC-based condensation model but that application of weights is questionable in condensing flows since the condensation significantly changes the gas flow.

Consider first the gas and particle properties along the nozzle axis. The gas translational temperature for the lowest and highest pressures under consideration is shown in Fig. 5. Here, $X = 0$ corresponds to the nozzle throat. As expected, the water nucleation results in a noticeable increase in gas temperature due to condensation. For the 1.577 bars case, the temperature in the plume region is up to 30 K higher when the condensation is included, which is comparable to the magnitude of the temperature in the noncondensing flow. The small temperature increase at about 0.25 mm is related to the compression wave that originates near the nozzle throat and propagate to the nozzle axis. It is present both in the condensing and noncondensing flow, and the location is nearly the same since the impact of the condensation is not very significant at this point.

For the 8.307 bars case, the influence of the condensation is obvious almost immediately after the nozzle throat (the temperatures start to deviate after the first $100 \mu\text{m}$ from the throat), and in the plume the gas temperature is several times higher in the condensing flow. Some statistical scatter is seen in this figure, where instantaneous gas properties are presented (an interpolation procedure was used here to smooth the results). The instantaneous properties are dependent on current cluster properties, and the use of only a finite number of simulated clusters contributes to their scatter. The higher temperatures in the nozzle for the condensing flow cause the

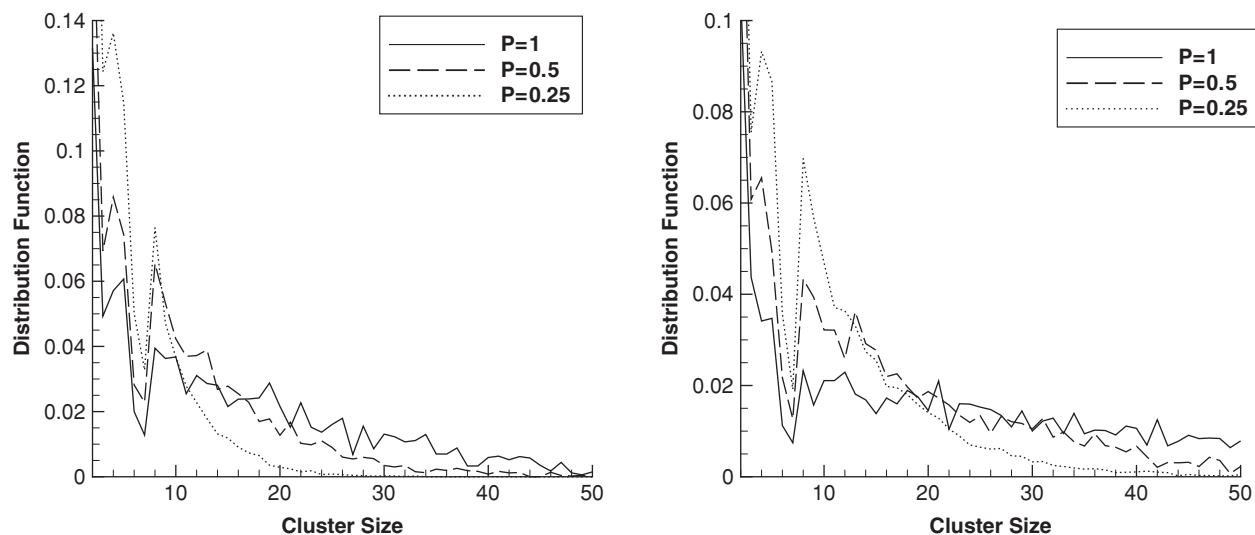


FIG. 6. Computed cluster size distributions for different coalescence probabilities P at $p_0 = 1.577$ bars (left) and $p_0 = 2.173$ bars (right).

formation of a compression wave near the nozzle lip, that propagates downstream and reflects at the axis at $X \approx 12$ mm. This results in a significant rise in gas temperature.

Consider now the terminal cluster size distributions at different stagnation pressures. Note first that there are several important properties that strongly affect the size distributions, among which are the evaporation heat, heat capacity, monomer sticking, and cluster coalescence probabilities. The first two of these properties are mostly functions of the cluster size, and the latter two, being characteristics of binary collisions, depend on the cluster sizes, internal energies, and relative collision velocities. The use of a constant coalescence probability in this work is a significant oversimplification of the actual cluster collision process, primarily related to the lack of information on collisions of small clusters. While the coalescence probability of two relatively large clusters (100-mers and larger) may be reasonably assumed to be close to the unity for Weber numbers on the order of 1, the coalescence of smaller clusters is less likely and for

the limiting case of dimer collisions may approach that of monomer sticking, which is about 0.2 for water.

The numerical analysis has shown that the size distribution significantly depends on the coalescence probability, see Fig. 6. The increase in the coalescence probability from 0.25 to 1 results in a significant redistribution of cluster sizes and a shift from smaller sizes to larger ones. Such a trend is expected, since a higher coalescence probability at a given collision rate increases the population of large clusters. Although the coalescence is accompanied by energy release from the electron structure of smaller clusters to the internal energy of larger clusters, the larger internal energy is then redistributed over a significantly larger number of internal degrees of freedom. The resulting gas temperatures were, therefore, found not to change noticeably with the coalescence probability.

Comparison of the computed and experimental cluster size distributions¹⁸ for these pressures is presented in Fig. 7. Since the dimers were not measured in Ref. 18; hereafter, the experimental points were normalized to match the population

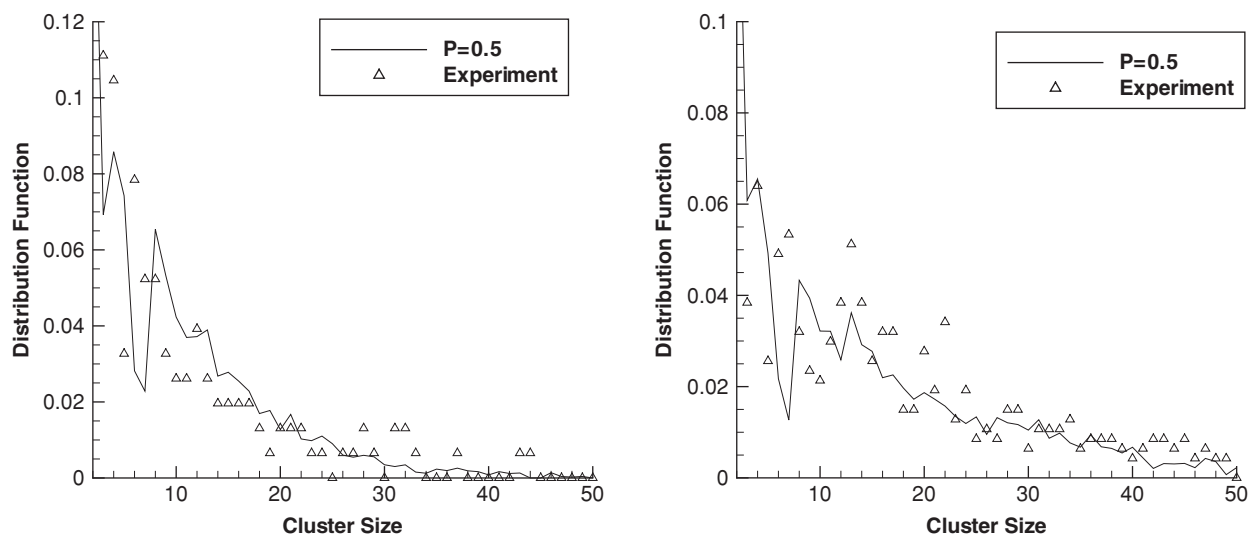


FIG. 7. Terminal cluster size distributions for $p_0 = 1.577$ bars (left) and $p_0 = 2.173$ bars (right): comparison with data (Ref. 18).

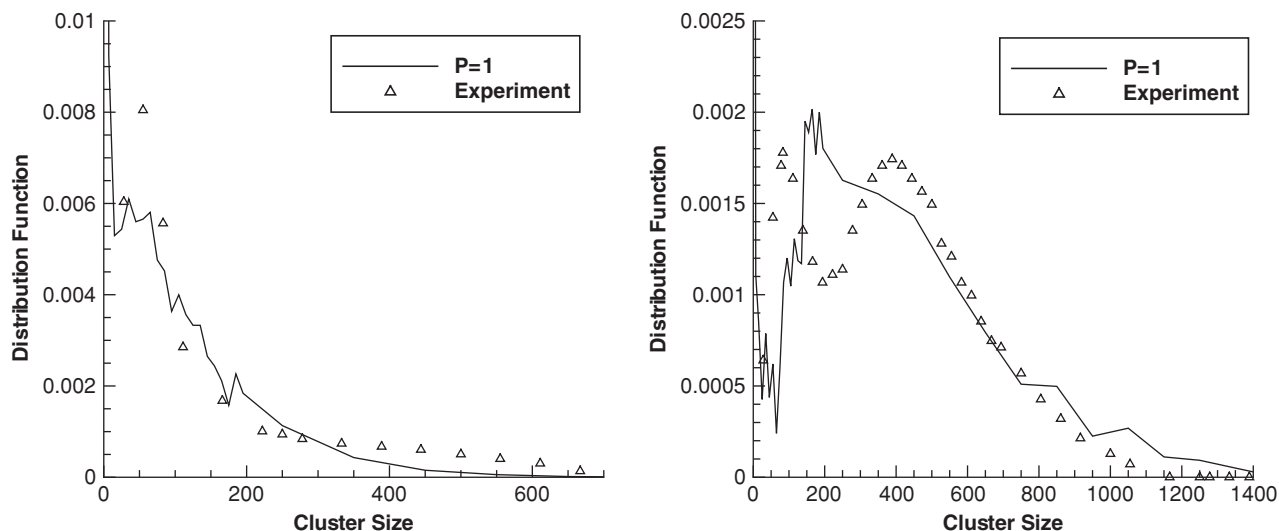


FIG. 8. Terminal cluster size distributions for $p_0 = 5.144$ bars (left) and $p_0 = 8.307$ bars (right): comparison with data (Ref. 18).

of the computed clusters excluding dimers. The case with a coalescence probability of 0.5 gives better agreement with the data and is, therefore, shown here. It needs to be mentioned that the local minimum observed for 6-mers and a local maximum observed for 8-mers are not statistical fluctuations, but the consequence of the corresponding minimum and maximum in the cluster evaporation energies. Note that for $p_0 = 1.577$ bars, the best agreement with the data would produce a computation that utilizes a constant coalescence probability between 0.25 and 0.5, whereas for $p_0 = 2.173$ bars, a larger coalescence probability between 0.5 and 1.0 would produce a better agreement. This is reasonable, since higher pressures are generally characterized by higher degree of nucleation and larger cluster sizes, for which the coalescence probability is expected to increase.

For the two largest pressures under consideration, the computations with a coalescence probability of 1 provide better agreement with the data, and the corresponding results are shown in Fig. 8. For $p_0 = 5.144$ bars, the computed location of the second maximum in the distribution function agrees well with the corresponding experimental value, although the population of such clusters is somewhat higher in the experiments. The most noticeable difference is observed in the large cluster tail, where clearly more clusters were observed in the experiment. In the calculation, the large cluster tail is closer to the lognormal shape. Interestingly, the situation is opposite for $p_0 = 8.307$ bars, for which the tail is somewhat more populated in the numerical prediction. More importantly, the

numerical results do not produce a clear bimodal structure at this pressure. Although this is clearly related to some approximations used in the model, more research is needed to single out the most important reason for this. The average cluster sizes for the above computation versus experiment comparisons are summarized in Table I. There is reasonable agreement between the results, especially for the three lowest pressures.

V. CONCLUSIONS

A new method for modeling homogeneous condensation is presented, based on the Eulerian description of the gas phase coupled with the Lagrangian approach to the cluster phase formation. A continuum, Euler/Navier–Stokes solver VAC is used to model the gas transport, and a kinetic particle solver is developed in this work to simulate cluster nucleation and growth. Conservation of mass, momentum, and energy is enforced through a two-way coupling, with gas properties influencing the cluster evolution through the dimer formation and monomer–cluster collisions (both elastic and inelastic), and mass, momentum, and energy transfer from the cluster to the gas phase handled via source terms in the continuum equations. The proposed approach is orders of magnitude faster than a comparable approach based on the DSMC method. Note also that it may easily be extended to model heterogeneous condensation.

The following cluster-related processes are taken into account in the kinetic solver: (i) collisional dimer formation that uses theoretical temperature-based dimer formation rates defining the number of dimers created in each cell per time step, (ii) elastic monomer–cluster collisions that change the translational and internal energies of colliding particles, with energy transfer modeling using the Larsen–Borgnakke model, (iii) inelastic monomer–cluster collisions that result in monomer sticking, (iv) cluster–cluster coalescence simulated with a conventional DSMC collision algorithm based on the majorant frequency scheme, and (v) evaporation of monomers from clusters based on the RRK model.

TABLE I. Average computed and measured cluster sizes at different pressures.

Stagnation pressure (bars)	Computed	Measured
1.577	12	9
2.173	18	20
5.144	107	80
8.307	417	338

The new model was found to reproduce the well known theoretical dimer formation equilibrium constants for the two gases under consideration, argon and water. Water nozzle expansion was modeled with the stagnation pressure ranging from 1.5 to 8.3 bars, which corresponds to the average cluster size increasing from below 10 to over 300. The results on the terminal cluster were found sensitive to the cluster coalescence probability, with the average cluster size increasing significantly when this probability was increased from 0.25 to 1. Comparisons with available experimental data have shown good agreement at lower pressures, and somewhat worse agreement at the highest pressure under consideration, where no visible bimodal size distribution structure was noticed in the calculations.

ACKNOWLEDGMENTS

The authors are extremely thankful to Professor Udo Buck for his support and patience in explaining experimental setup and data, and providing additional data on cluster size distributions, Dr. Matthew Braunstein for his help with the water binding energy analysis, and Dr. Y. Scribano for providing additional data for the water dimer equilibrium constant and heat capacity. The work was supported by the Air Force Office of Scientific Research.

- ¹F. S. Simmons, *Rocket Exhaust Plume Phenomenology* (The Aerospace Corporation Aerospace Press Series, AIAA, El Segundo, CA, 2000).
- ²R. T. V. Kung, L. Cianciolo, and J. A. Myer, *AIAA J.* **13**(4), 432 (1975).
- ³L. Prandtl, *Atti del Convegno Volta* (Reale Accademia D'Italia, Rome, 1936).
- ⁴X. Luo, G. Lamanna, A. P. C. Holten, and M. E. H. van Dongen, *J. Fluid Mech.* **572**, 339 (2007).
- ⁵F. Abraham, *Homogeneous Nucleation Theory: The Pretransition Theory of Vapor Condensation* (Academic, New York, 1974).
- ⁶J. E. McDonald, *Am. J. Phys.* **31**, 31 (1963).
- ⁷E. R. Perrell, W. D. Erickson, and G. V. Candler, *J. Thermophys. Heat Transfer* **10**(2), 277 (1996).
- ⁸A. G. Gerber, *J. Fluids Eng.* **124**, 465 (2002).
- ⁹J. Qian, Z. Han, and L. An, in *Proceedings of the Third IEEE Conference on Industrial Electronics and Applications* (IEEE, Piscataway, NJ, Singapore, 2008), Vol. 720.
- ¹⁰G. Gyarmathy, in *Condensation in Flowing Steam, Two-Phase Steam Flow in Turbines and Separators*, edited by M. J. Moore and C. H. Sieverding (Hemisphere, Washington, DC, 1976), Vol. 127.
- ¹¹J. D. Chenoweth, K. W. Brinckman, J. J. York, G. Feldman, and S. M. Dash, "Progress in Modeling Missile Fuel Venting and Plume Contrail Formation," AIAA Paper No. 2007-1012, 2007.
- ¹²D. P. Brown, J. Jokiniemi, and T. Valmarin, *J. Aerosol Sci.* **28**, S323 (1997).

- ¹³S. G. Rubin and J. C. Tannehill, *Annu. Rev. Fluid Mech.* **24**, 117 (1992).
- ¹⁴J. Pudykiewicz, A. Kallaur, and P. Smolarkiewicz, *Tellus* **48**(3), 231 (1997).
- ¹⁵R. Paoli, T. Poinso, and K. Shariff, in *Proceedings of the 2006 Summer Program, Center for Turbulence Research, NASA* (Ames/Stanford University, Stanford, CA, 2006).
- ¹⁶J. Zhong, M. Zeifman, S. Gimelshein, and D. Levin, *AIAA J.* **43**(8), 1784 (2005).
- ¹⁷G. A. Bird, *Molecular Gas Dynamics and the Direct Simulation of Gas Flows* (Clarendon, Oxford, 1994).
- ¹⁸C. Bobbert, S. Schutte, C. Steinbach, and U. Buck, *Eur. Phys. J. D* **19**, 183 (2002).
- ¹⁹A. Itkin and E. Kolesnichenko, *Microscopic Theory of Condensation in Gases and Plasma* (World Scientific, Singapore, 1997).
- ²⁰H. Hettema and J. McFeaters, *J. Chem. Phys.* **105**, 2816 (1996).
- ²¹J. Soler, N. Garcia, O. Echt, K. Sattler, and E. Recknagel, *Phys. Rev. Lett.* **49**, 1857 (1982).
- ²²S. Toxvaerd, *J. Chem. Phys.* **115**, 8913 (2001).
- ²³M. I. Zeifman, J. Zhong, and D. A. Levin, "A Hybrid MD-DSMC Approach to Direct Simulation of Condensation in Supersonic Jets," AIAA Paper No. 2004-2586, 2004.
- ²⁴J. Zhong, M. Zeifman, and D. Levin, *J. Thermophys. Heat Transfer* **20**(1), 41 (2006).
- ²⁵A. Gallagher-Rogers, J. Zhong, and D. A. Levin, "Simulation of Homogeneous Ethanol Condensation in Supersonic Nozzle Flows Using DSMC," AIAA Paper No. 2007-4159, 2007.
- ²⁶J. Zhong and D. Levin, *AIAA J.* **45**(4), 902 (2007).
- ²⁷B. Briehl and H. Urbassek, *J. Vac. Sci. Technol. A* **17**(1), 256 (1999).
- ²⁸S. Gratiy, J. Zhong, and D. A. Levin, "Numerical Simulation of Argon Condensation with a Full Kinetic Approach in a Free-Expanding Jet," AIAA Paper No. 2006-3598, 2006.
- ²⁹R. D. Levine, *Molecular Reaction Dynamics* (Cambridge University Press, Cambridge, England, 2005).
- ³⁰R. Jansen, I. Wysong, S. Gimelshein, M. Zeifman, and U. Buck, *J. Chem. Phys.* **132**, 244105 (2010).
- ³¹N. Gimelshein, S. Gimelshein, and A. Ketsdever, "Thrust Augmentation in Solid Rocket Motors Using Beamed Microwave Energy," AIAA Paper No. 2009-4962, 2009.
- ³²G. Toth, *Astrophys. Lett. Commun.* **34**, 245 (1997).
- ³³C. Borgnakke and P. S. Larsen, *J. Comput. Phys.* **18**, 405 (1975).
- ³⁴S. Chapman and T. J. Cowling, *The Mathematical Theory of Non-uniform Gases* (Cambridge University Press, Cambridge, England, 1991).
- ³⁵J. Zhong, M. I. Zeifman, and D. A. Levin, *J. Thermophys. Heat Transfer* **20**(3), 517 (2006).
- ³⁶J. F. Crifo, *Icarus* **84**, 414 (1990).
- ³⁷M. Zeifman, B. J. Garrison, and L. V. Zhigilei, *J. Appl. Phys.* **92**, 2181 (2002).
- ³⁸Y. Okada and Y. Hara, *Eurozoru Kenkyu* **22**(2), 147 (2007).
- ³⁹N. Ashgriz and J. Y. Poo, *J. Fluid Mech.* **221**, 183 (1990).
- ⁴⁰M. S. Ivanov and S. V. Rogasinsky, *Sov. J. Numer. Anal. Math. Model.* **2**(6), 453 (1998).
- ⁴¹R. Kalus, *J. Chem. Phys.* **109**(19), 8289 (1998).
- ⁴²P. S. Dardi and J. S. Dahler, *J. Chem. Phys.* **93**(5), 3562 (1990).
- ⁴³Y. Scribano, N. Goldman, R. J. Saykally, and C. Leforestier, *J. Phys. Chem. A* **110**(16), 5411 (2006).
- ⁴⁴S. Schütte and U. Buck, *Int. J. Mass. Spectrom.* **220**, 183 (2002).